VOL. 9, NO. 3, MARCH 2014 ISSN 1819-6608
ARPN Journal of Engineering and Applied Sciences


www.arpnjournals.com

A CFD INVESTIGATION ON FLUID DYNAMIC GAUGING

R. Thundil Karupparaj, Bharani Kumar K. V. and M. P. Dhyan Shankar
School of Mechanical and Building Sciences, VIT University, Vellore, India
E-Mail: thundil.rajagopal@vit.ac.in

ABSTRACT

This study deals with computational fluid dynamics (CFD) of fouling inside tubes or passages. These cases arise in present industrial situations involving fluid flows inside. The investigation on fouling is carried out by the technique called fluid dynamic gauging (FDG), which is a non-contact technique for measuring the thickness of soft deposit layer on solid surfaces immersed in liquid environment in situ and in real time. Laminar Newtonian flow has been investigated with Reynolds number at the nozzle throat in the range $116<Re_t<930$ and with the flow velocity of 0.0015 m/s to 0.124 m/s with water as the working fluid. The 3-dimensional model is created using SOLIDWORKS software. The fluid domain is discretized using finite volume method using ICEMCFD12.1 pre-processing tool. Both hexahedral and tetragonal mesh is generated which is used to capture the hydrodynamic boundary layers. The flow field through the 3-dimensional domain is captured by solving the appropriate governing equations namely conservation of mass and momentum equations. The convergence criteria are set to 10E-04 for mass and momentum. The numerically predicted results are compared with the experimental data available in the literature and a very good agreement exists between the two. Fouling phenomenon is calculated by finding the pressure difference between inlet and gauge tube outlet.

Keywords: fluid dynamic gauging (FDG), computational fluid dynamics (CFD), laminar Newtonian flow, fouling, soft deposits.

1. INTRODUCTION

Fouling is generally defined as the accumulation or deposition of the unwanted materials on the surfaces of processing equipment. The major problem in oil, food, water and petrochemical industries is the formation of fouling layers caused by undesired attachment and accumulation of materials from the process industries. Hence, understanding the mechanisms of accumulation of unwanted materials and its proper cleaning is critical in developing effective mitigation and cleaning methods, but this requires many sensors and monitoring techniques for identifying the attributes of fouling such as thickness and rheology.

The great challenge is the direct measurement of the thickness of soft foulant layers in a flowing liquid, which can be achieved for several applications by using the technique called fluid dynamic gauging (FDG) developed by Tuladhar *et al*., [1]. The advantages of FDG are as follows (i) it is a non-contact technique; (ii) measurements can be made rapidly in situ and in real time; and (iii) The knowledge of material parameters is not required, but the limitation is that the foulant layer is assumed to be stiff i.e., it does not change shape while exposed to the forces imposed by the gauging liquid flow during the measurement. If the gauging flow causes deformation, the mode and extent of this deformation can be used to determine the strength of the layer by the observations with computational fluid dynamics (CFD) simulations of the normal and shear stresses acting on the foulant layer (Chew *et al*., [2]).

During measurements in the FDG method, the nozzle must be close enough to the film surface, i.e. $h/d_t \leq 0.25$. The clearance between the nozzle and the foulant layer is larger than the width of the nozzle which suggests that the prediction of results based on the lubrication approximation should provide useful results [3] when combined with the laminar nature of the flow. This approach was employed by Chew *et al*. and later by Gu *et al*., [4] to estimate the shear stress imposed on the surface. In both cases shear stress distributions obtained from CFD simulations showed good agreement with the analytical solution for a radial flow between two parallel disks obtained by Middleman (1998) using lubrication theory.

Studies such as that by Chew *et al*., [5] have shown that FDG could also be used to quantify the strength of soft deposits. The gauge employs flows in the laminar regime, allowing computational fluid dynamics (CFD) to be used to give reliable estimates of the flow field and stress distribution in the flow. Chew *et al*., [6] quantified the strength of different tomato paste layers by measuring the deformation of the film following gauging at a known shear stress exerted by the gauge on the film. Thickness measurements were made at high clearance (low shear stress) and following exposure of the film to higher shear stresses induced by moving the nozzle closer to the film.

The stresses induced on the film by the gauging flow are determined by the liquid flow rate, clearance and also the external geometry of the nozzle. Peralta *et al*., [3-10] demonstrated how the external shape of the nozzle could affect, very noticeably, the shear stress and pressure profiles on a gauged surface. They identified geometries that produced interesting shear stress and pressure profiles such as linear, peaked or bimodal distributions. These types of profiles are attractive to FDG operation as they offer the opportunity to manipulate the forces exerted on a film by simply changing the nozzle. For example, an approximately constant erosion of the film can be produced under the nozzle rim when an even shear stress profile is used. Alternately, another shape could yield high sensitivity to clearance (measurement precision) while minimizing fluid shear.

This paper compares the results obtained in T. Gu *et al*., for the experimental results with the simulations

results obtained in ANSYS CFX 12.1. It is found that the previous work has been made for the simulation for h/d_t = 0.06. As a result in this work the simulation is done for ratios, h/d_t = 0.1, 0.15, 0.2, 0.25 for four different Reynolds's numbers, i.e., Re_{duct} = 116, 474, 625 and 960 and Re_{tube} = 49, 305, 430 and 537 to find the pressures obtained at the gauge outlet and also its conformity with the results obtained in experiments.

2. PRINCIPLES OF FDG

Figure-1 illustrates the principles of the dynamic gauging technique. A nozzle of throat diameter d_t is connected to a tube of inner diameter d. The nozzle is fully immersed in a liquid (in this case a filled duct of square cross-section), and positioned close to but not touching the gauged surface. There are two pressure driving forces [11] operating: (i) a fixed hydrostatic suction head, and (ii) a pressure head associated with flow in the duct. These constitute a pressure difference which induces fluid to flow into the nozzle.

The discharge liquid is collected and weighed. The discharge mass flow rate m is sensitive to the nozzle clearance ratio h/d_t, as shown in Figure-2. The working range of the gauge is in the incremental zone, $h/d_t<0.25$, where m is usefully responsive to the value of h. Beyond h/d_t = 0.25 the mass flow rate is insensitive, hence h/d_t = 0.25 van be considered as the upper working limit of fluid dynamic gauging. The prime assumption made is that the surface being studied is relatively stiff and impermeable. Therefore measurement of m may be used to infer h, and subsequently any change in has a result of deposition or cleaning.

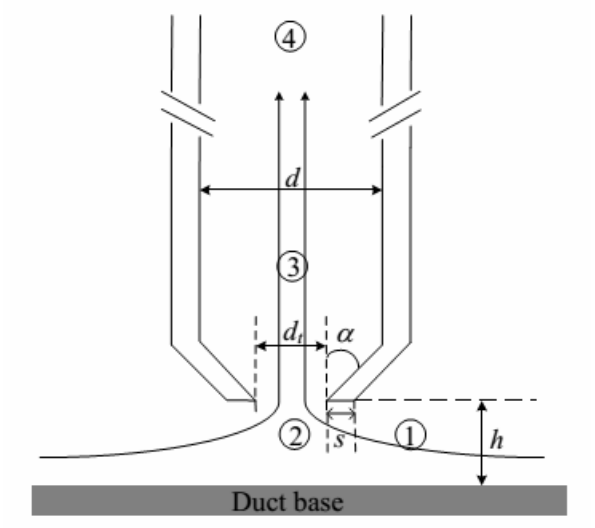

Figure-1. Schematic of fluid dynamic gauging [3].

The discharge coefficient, Cd, is used to quantify the performance of the nozzle. C_d accounts for the energy losses due to the flow near the nozzle entrance, and is defined as the ratio of the actual to ideal mass flow rate through the nozzle, viz.

$$C_d = \frac{m_{actual}}{m_{ideal}} = \frac{m}{\frac{\pi d_t^2}{4}\times\sqrt{(2\Delta p_{13})}} \quad (1)$$

Where

$$\Delta p_{13} = \Delta p_{14} - \Delta p_{34} = \rho g H + p_s - \frac{128\mu m l_{eff}}{\pi d^4 \rho} \quad (2)$$

Here, p_s is the static gauge pressure in the duct, H is hydrostatic head, as shown in Figure-2(a) (with H» D), and subscripts 1, 3 and 4 refer to various stations in the tube as shown in Figure-1. l_{eff} is the equivalent length of the tube, allowing for frictional losses caused by the two right-angle bends (Figure-2(b))

3. EXPERIMENTAL

The experimental data provided in the paper T. Gu *et al*., was used as reference. The geometry was created as given in the work. The details on the geometry are as given in the paper.

Figure-2 shows a schematic of the duct flow apparatus. The working fluid was water at 20°C and approximately 1 atm. A gauging nozzle with d_t = 1 mm, d = 4 mm, s = 1 mm and α = 45° was located in a duct of side D = 15 mm and length L = 248 mm. The duct was constructed from Perspex with a 450 mm (30D) entry section to ensure fully developed flow. The mean velocity through the duct was in the range 0.0015 - 0.124 m/s (Re_{duct} 116 - 930). The gauge was positioned with its centreline on the central vertical plane of the duct, 70 mm from the entrance. The clearance between the gauging surface at the base of the duct and the nozzle was adjusted by a micrometer (resolution ± 2 μm). The nozzle approaches the gauging surface in advancing mode, i.e. starting from $h/d_t \geq 1$. The discharge gauging flow was collected using an electronic balance (accuracy ± 0.05g).

The gauge was connected to a siphon tube of length l = 640 mm open to the atmosphere with H =307 mm. This fixed hydrostatic head provides the principal driving force for the gauging flow. The second driving force originates from the static gauge pressure in the duct, associated with the bulk flow. This duct static pressure was measured near the inlet using a pressure sensor (accuracy ± 34 Pa). The static gauge pressures ranged from 388 Pa (Re_{duct} = 116) to 17 200 Pa (Re_{duct} = 11 000).

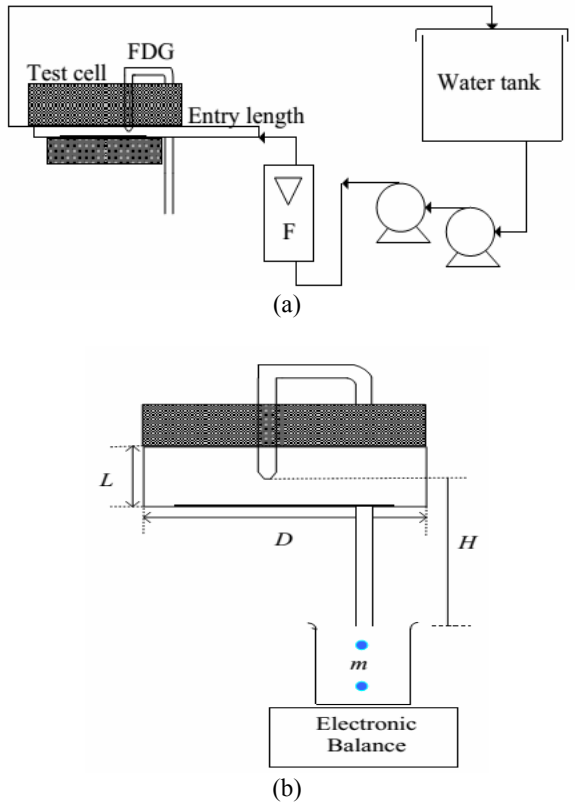

Figure-2. (a)Schematic of duct flow apparatus and (b) Test section [1].

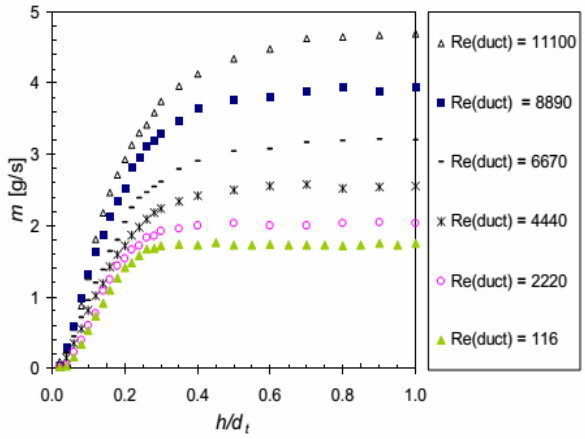

Figure-3. Variation of m against h/d_t [3].

The experimental analysis was done for Reynolds's number in the range $116 \leq Re_{duct} \leq 11100$. In the graph (Figure-3) actual mass flow rate m is plotted against h/d_t.

The graph for mass flow rate and h/d_t have two regions that is, incremental and asymptotic regions (Figure). The mass flow rate increases with h/dt values upto approximately $h/d_t = 0.25$ beyond which there is no effect of h/dt on the mass flow rate [1-9]. For most of the cases transition occurs in the range $0.25 \leq h/d_t \leq 0.3$.

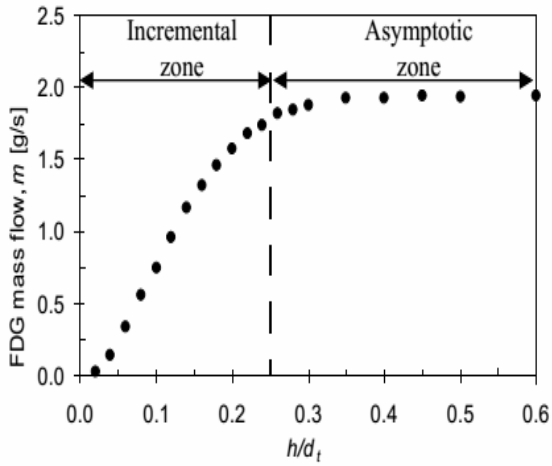

Figure-4. The working range of FDG for duct flow and the dotted line denotes the transition region [4].

4. CFD SIMULATIONS

4.1. Governing equations

CFD simulations for the flow are performed for cases where both the duct and gauging flows are in the laminar regime. The incompressible, steady-state, Navier-Stokes equations for a Newtonian liquid are imposed and solved with finite volume method (FVM) using ANSYS CFX 12.1 software package. The convergence criteria are set to 10E-04 for mass and momentum. The continuity and Navier-Stokes equations are:

Continuity:

$$\nabla . v = 0 \tag{3}$$

Navier-Stokes:

$$\rho v . \nabla v = -\nabla p + \mu \nabla^2 v + \rho g \tag{4}$$

Where v is the velocity vector, p is the pressure; ρ is the density, μ the dynamic viscosity and g the acceleration due to gravity which is set to zero in this case for computational convenience.

In the experimental situation pressure difference driving the flow is generated by a gravitational head. In the simulation, however, it proves convenient to neglect gravity within the flow field and instead simply to impose a certain pressure difference to drive the flow (Tritton, 1988).

4.2. Model geometry and boundary conditions

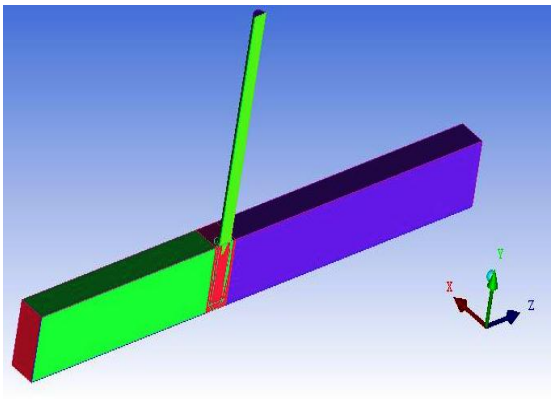

Figure-5. Geometry used for computation.

Figure-5 shows the geometry of the model created in accordance to the simulations dimensions. A suction tube is positioned with its axis perpendicular to the longitudinal axis of the duct. The working fluid (water) enters the duct in the z- directions, crossing the inlet plane and leaves through outlet plane (z-direction) and the gauging tube in the y-direction. In the experiments the mass flow rate at the duct inlet was regulated using a valve as measured using a rotameter. The hydrostatic head, H is set and the static pressure, p_s is established, the clearance h is fixed, and the gauge discharge flow rate, m is measured. In the simulations, the inputs are the velocities at the duct inlet, the gauge tube outlet and the pressure at the duct outlet; their values are all extracted from the experimental data. The output of the CFD simulation is the difference between the points 3 in the gauging tube and the duct outlet, i.e. Δp_{13}, which is used to calculate the coefficient of discharge C_d from Equation (1).

The boundary conditions are:

a) Duct inlet: fully developed laminar flow is assumed, so that the duct velocity varies by the velocity profile

$$w = \frac{16 \times w_{max}\{(x+0.5D)(D-(x+0.5D))\} \times \{y(D-y)\}}{D^4} \quad (5)$$

Where x and y are the width-wise and height-wise coordinates at the duct inlet plane; w_{max} is the maximum z-wise velocity being approximately equal to twice the mean z-wise velocity, w_{mean}. The value for w_{mean} was obtained from experimental data. The x and y-wise velocities i.e. u and v are set to zero

b) Gauging tube outlet: fully developed laminar flow is assumed giving the Hagen-Poiseuille velocity profile

$$v = v_{max}\left(1 - \left(\frac{r}{r_i}\right)^2\right) \quad (6)$$

Where r is the radial coordinate measured from the tube centreline, r_i is the inner radius of the tube, and v_{max} is the y-wise velocity on the tube centreline, being twice the mean velocity as calculated from experimental data. The x and y-wise velocities u and v are zero. The length of the tube described is taken in such a way that it ensures the flow to be fully developed: it varied with Re_{tube}, Re_{duct} and h/d_t, with typically $10<l/d_t<110$.

c) Duct outlet: the duct outlet was set sufficiently far downstream such that the flow line stabilizes and becomes parallel and normal to the plane. The value of L' was determined from trial and error; L'/D=11 was found suitable. u and v are set zero. The pressure is set to the (negative) static pressure, p_s measured in the experiments, i.e.

$p = -p_s = -414$Pa

d) Walls: the walls of the duct and the gauge tube (r_i = 2mm, r_o = 3mm), the walls of the nozzle were all modeled as impermeable (normal component of the velocity set to zero) with no slip.

e) Symmetry: no flow crosses the y-z plane of symmetry, thus n.v = 0 at x = 0, for all y and z

4.3. Meshing

The whole model is meshed using a hybrid mesh. Tetragonal mesh is used near the nozzle area and hexahedral mesh is used for other areas. This is done in order to reduce the errors caused in meshing near the nozzle area using hexahedral mesh. A higher concentration of computational elements was assigned near to the nozzle-surface clearance region beneath the nozzle as shown in the Figure-6. This is the region were the maximum velocity and pressure gradients can be encountered, so the mesh was refined in order to obtain the flow pattern and velocity - pressure values properly. The mesh was generated using ICEMCFD 12.1, the number of elements varied with h/d_t, l/d, L'/D, Re_{duct} and Re_{tube}. A computational domain [12-14] of the flow region is generated with total number of elements to be approximately440000 with solid domain around the nozzle.

In the previous studies by T. Gu *et al*., mesh densities were varied for different cases and it was found that unnecessary increase in the mesh densities resulted in increase of simulation time and a very slight improvement in results were obtained which could be ignored. A satisfactory solution took approximately 16minutes to solve in a computer having a CORE 2Duo 2.2GHz processor with 4GB RAM.

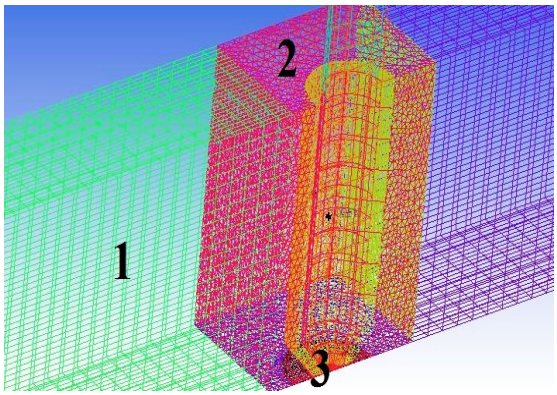

Figure-6. (1)Hexahedral mesh (2) Tetrahedral mesh (3) Refined mesh region underneath nozzle.

5. RESULTS AND DISCUSSIONS

5.1. Streamlines

The streamline obtained from the simulation is as shown in the Figure. The Figure-7 suggests that the flow field can be divided into three regions, namely;

a) Undisturbed flow region, far from the nozzle
b) The suction region around the nozzle mouth and
c) The recirculation region within the nozzle

On inspection it was found that the flow region far from the nozzle has the same flow pattern and only the regions (ii) and (iii) varied. This result indicates the unimportance of the flow approximations made far from the nozzle. The flows are predominantly axial in the undisturbed flow region. The flow changes from axial to radial convergent flow as it approaches the nozzleentrythat is the suction region, in which the flow is radial and sensitive to Re_t, h and s. After the flow enters the nozzle, downstream to the suction region flow diverges in the nozzle throat generating recirculation.

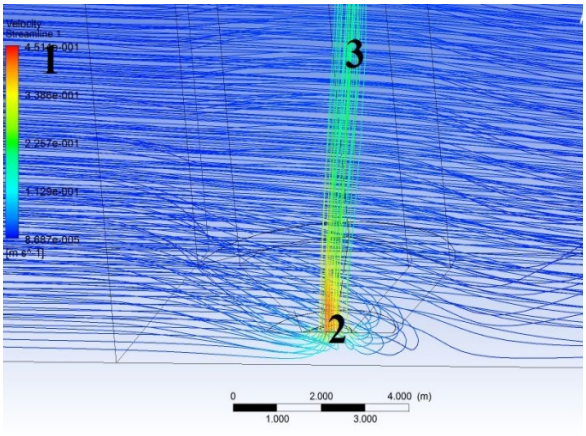

Figure-7. (1)Undisturbed flow region (2) suction region (3) Recirculation region.

5.2. Flow behaviour

Figure-8 shows the selected set of streamlines in the duct and the gauge tube for (h/d_t = 0.2, Re_{duct} = 930, Re_{tube} = 537). Streamline 1, near the base of the duct shows that, the flow was mainly z-wise in the duct but when approaching the lip of the nozzle the flow develops a vertical component. Streamline 2 shows the z-wise flow in the duct and the obstruction of the gauge tube as the duct flow passes it. It can be seen that the flow in the tube is asymmetric in the y-z plane until some distance above the nozzle throat due to the momentum from the duct flow. As Re_{tube} increases a longer gauging tube is required for the flow to be stabilized and to achieve a well-developed velocity profile in the tube.

Simulations were not performed for flows with Reynolds number higher than Re_{duct}> 930, as the flow is likely to feature eddy separation (behind the gauging nozzle), instabilities (divergent flow within the gauging nozzle) and laminar- turbulent transition inside the nozzle.

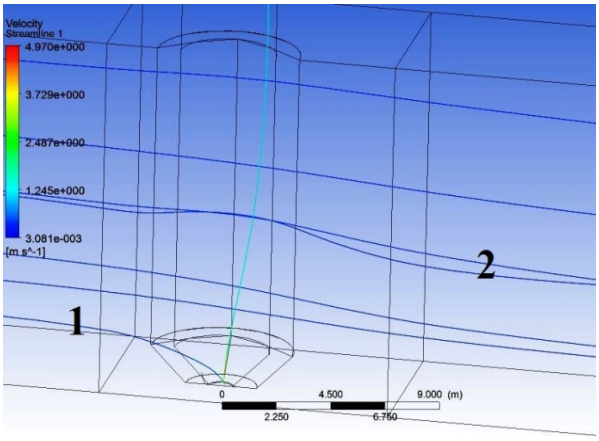

Figure-8. (1) Streamline entering nozzle (2) Streamline past the nozzle.

5.3. Coefficient of discharge

In the CFD simulations Δp_{13} is calculated by adding the static gauge pressure to the tube outlet pressure (output from the CFD simulation). Δp_{13} is then used to calculate C_d with the Equation (1). Figure-10 compares the C_d values obtained from the simulations for different duct flows (Re_{duct} = 116,465, 625 and 930; Re_{tube} = 49, 305, 430 and 537). The loci plotted for the simulation results are obtained by interpolation. The agreement between the present CFD simulation and those done by T. Gu *et al*., is entirely satisfactory to within 8% and lies with the bounds of simulation error.

Previously simulation is made for h/d_t= 0.06 at Re_{duct} = 116 and Re_{tube} = 49. The table shows the input parameters used in the simulation work and that used in the experimental work.

Table-1. Effective flow and geometrical parameters.

	Present work	**Experimental [1]**
Hydrostatic head, H (mm)	307	320
Static pressure, p_s (Pa)	414	1006
Duct Reynolds number, Re_{duct}	116, 465, 625, 930	474
Effective length, l_{eff} (m)	0.65	1.20
Nozzle tip width, s (mm)	1	0.5

The graph (Figure-9) shows the comparison between the previous work and the present simulation work. Since there is good agreement between the results obtained, the simulation work has been done for different h/d_t and Reynolds numbers as shown in the graphs (Figure-10 (a)-(d)). The C_d value increases upto $h/d_t = 0.2$ and beyond which the values decreases by 0.01 and it gets insensitive. As the Reynolds number increases the associated static pressure increases.

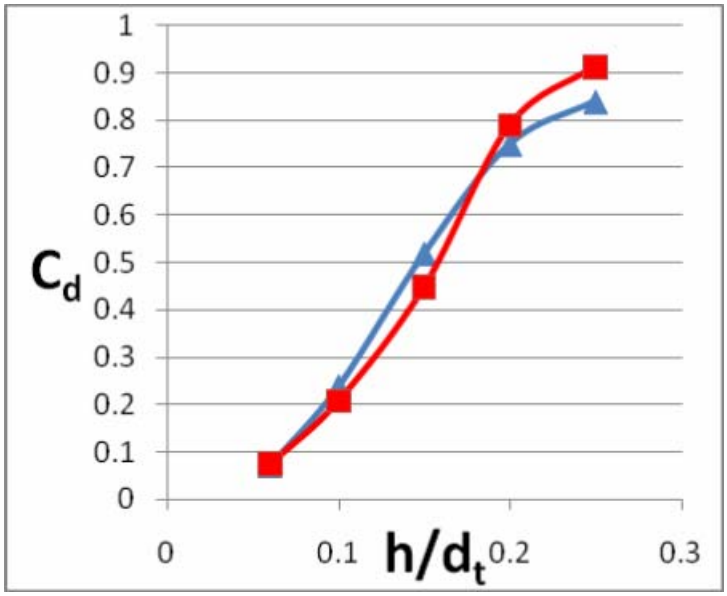

Figure-9. Variation of C_d with h/d_t.

For a given Reynolds number C_d increases as h/d_t increases upto $h/d_t = 0.2$. This implies that the total pressure loss near the constriction is significant. Therefore, it can be concluded that lower C_d values is mainly due to the larger pressure drop under the nozzle rim.

Since, C_d starts to moderate after $h/d_t = 0.2$ it can be recommended that $h/d_t = 0.2$ can be set as the upper working limit for both CFD simulation as well as experimental purpose. When the nozzle is far from the test surface ($h/d_t>0.25$) the presence of fouling layer has little effect on C_d

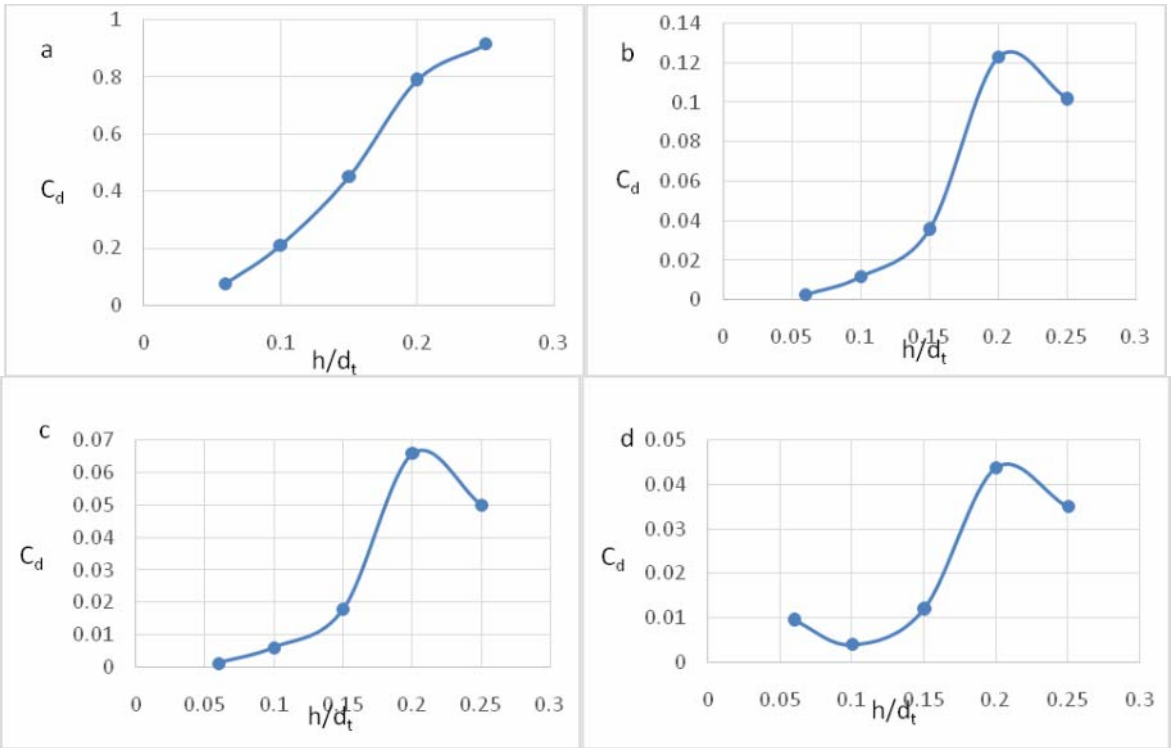

Figure-10. C_d vs h/d_t for (a) Re_{duct} = 116, Re_{tube} = 49 (b) Re_{duct} = 65,Re_{tube} = 305 (c) Re_{duct} = 625,Re_{tube} = 430 (d) Re_{duct} = 930, Re_{tube} = 537.

Simulations and measurements show excellent agreement and the assumptions made in the model, particularly that of laminar flow through the complete flow field are satisfactory.

Table-2. Comparison among present and previous C_d values.

h/d_t	C_d(previous work)	C_d (present work)	% error
0.06	0.0725	0.076	5.26
0.1	0.24	0.21	12.50
0.15	0.52	0.45	13.46
0.2	0.75	0.79	5.06
0.25	0.84	0.91	7.60

CONCLUSIONS

The technique of fluid dynamic gauging has been demonstrated using CFD tool ANSYS CFX12.1 for steady, incompressible, laminar flows for $116 \leq Re_{duct} \leq 930$ and $49 \leq Re_{tube} \leq 537$. The numerical result has good agreement with the experimental work [3] within 8% approximately thereby supporting the validity of the work and the assumptions considered.

Hence, CFD can be used as a tool for fluid dynamic gauging to determine the deposit characteristics in the duct or channel flows. Application of this knowledge to study the flow through duct showing fouling can be extended to annular duct and also with different nozzle dimensions and geometries.

ACKNOWLEDGEMENT

We wish to acknowledge the expertise of Mr. Balaji Ranganathan from FL Smidth, CFD Division, and Chennai for his valuable suggestion in carrying out this work.

REFERENCES

[1] Investigation of alkaline cleaning-in-place of whey protein deposits using dynamic gauging (2002) by T.R Tuladhar, W.R Paterson, D.I Wilson, and Institution of chemical engineers. Vol. 80, Part C.

[2] CFD studies of dynamic gauging (2004) by J.Y.M Chew, S.S.S Cardoso, W.R Paterson, D.I Wilson, Chemical Engineering Science.

[3] An analytical method for selecting the optimal nozzle external geometry for fluid dynamic gauging (2011) by J.M Peralta, Y.M.J Chew, D.I Wilson, Chemical Engineering Science.

[4] Experimental and CFD studies of fluid dynamic gauging in duct flows (2009) by T. Gu, Y.M.J Chew, W.R Paterson, D.I Wilson, Chemical Engineering Science.

[5] Development of the scanning fluid dynamic gauge (2009) by P.W Gordon, Y.M.J Chew, D.I Wilson, International conference on heat exchanger fouling and cleaning.

[6] A fluid dynamic gauging device for measuring fouling deposit thickness in opaque liquids at elevated temperature and pressure (2013) by A. Ali, G.J Chapman, Y.M.J Chew, T. Gu, W.R Paterson, D.I Wilson, Experimental thermal and fluid science.

[7] Fluid dynamic gauging in duct flows - experiments and CFD simulations (2007) by T. Gu, Y.M.J Chew, W.R Paterson, D.I Wilson, International conference on Heat Exchanger fouling and cleaning.

[8] Application of fluid dynamic gauging to annular test apparatuses for studying fouling and cleaning (2011) by T, Gu, F. Albert, W. Augustin, Y.M.J Chew, M. Mayer, W.R Paterson, S. Scholl, L. Sheikh, K. Wang, D.I Wilson, Experimental thermal and fluid science.

[9] Pressure mode fluid dynamic gauging for studying cake build-up in cross-flow microfiltration (2011) by Vincent Y. Lister, Claire Lucas, Patrick W. Gordon, Y.M J. Chew, D.I Wilson, Journal of membrane science.

[10] Studies into the swelling of gelatin films using a scanning fluid dynamic gauge (2010) by Patrick W. Gordon, Anju D.M Brooker, Y.M J Chew, D.I Wilson, David W. York, Food and bioproducts processing.

[11] Fluid dynamic gauging for measuring the strength of deposits (2004) by J.Y.M Chew, W.R Paterson, D.I Wilson, Journal of Food Engineering.

[12] Premixed charge compression ignition in a direct injection diesel engine using CFD by R. Manimaran, R. ThundilKaruppa Raj, K. Senthil Kumar, WSEAS transaction on heat and mass transfer.

[13] Experimental study of recirculating flows indeuced by vane swirler (2009) by R. ThundilKaruppa Raj, V Ganesan, India Journal of engineering and material sciences.

[14] Experimental and parametric study of extended fins in the optimization of internal combustion engine cooling using CFD by J. Ajay Paul, Sagar Chavan Vijay, U. Magarajan, R. ThundilKaruppa Raj.